Distortion of the Three-Dimensional Structure of the vnd/NK-2 Homeodomain Bound to DNA Induced by an Embryonically Lethal A35T Point Mutation‡

Kae-Jung Hwang,[§,||,⊥] Bosong Xiang,[§,⊥,@] James M. Gruschus,[§] Ky-Youb Nam,[||] Kyoung Tai No,[||,+] Marshall Nirenberg,[#] and James A. Ferretti*[,§]

Laboratory of Biophysical Chemistry, National Heart, Lung and Blood Institute, National Institutes of Health, Bethesda, Maryland 20892-8013, Computer Aided Molecular Design Research Center, Soong Sil University, 1-1 Sangdo 5 Dong, Dongjak-gu, Seoul 156-743, Republic of Korea, and Laboratory of Biochemical Genetics, National Heart, Lung and Blood Institute, National Institutes of Health, Bethesda, Maryland 20892-4036

Received May 8, 2003; Revised Manuscript Received August 12, 2003

ABSTRACT: The three-dimensional solution structure obtained by NMR of the A35T mutant vnd/NK-2 homeodomain bound to the vnd/NK-2 consensus 16 bp DNA sequence was determined. This mutation to threonine from alanine in position 35 in helix II of the vnd/NK-2 homeodomain is associated with early embryonic lethality in *Drosophila melanogaster*. Although the unbound mutant protein is not structured, in the DNA-bound state it adopts the three-helix fold characteristic of all known homeodomains, but with alterations relative to the structure of the wild-type analogue. These structural modifications occur, and are accompanied by a 50-fold reduction in the DNA binding affinity, even though most of the protein−DNA interactions originally seen for the wild-type homeodomain are found likewise in the threonine analogue. Alterations include torsional angle changes in the loop between helix I and helix II, and in the turn between helix II and helix III, as well as in a distortion of the usual antiparallel orientation of helix I with respect to helix II. The alteration of the position of leucine 40 in the A35T mutant is proposed to explain the observed 1.27 ppm upfield shift of the corresponding amide proton resonance relative to the value observed for the wild-type analogue. A detailed comparison of the structures of the mutant A35T and wild-type vnd/NK-2 homeodomains bound to the cognate DNA is presented. The consequences of the structural alteration of the DNA-bound A35T mutant vnd/NK-2 protein may constitute the basis of the observed early embryonic lethality.

The homeobox gene is important in specifying positional information and segmental identity in the commitment of embryonic cells to specific pathways of development (*1*−*3*). Homeobox-containing genes are believed to act as master controlling genes both spatially and temporally. They are known to control genes that are important in the development of various organs such as the heart, thyroid, kidneys, eyes, and prostate in many organisms (*4*−*6*). The homeodomain is the highly conserved structural domain of a class of proteins that are encoded by the homeobox gene and function as regulators of transcription, at least in part, by specifically binding to DNA (*7*). The ability of the homeodomain to adopt a three-dimensional structure and to properly bind a specific sequence or set of sequences of DNA depends on the nature of the amino acid residues in specific positions within the three-dimensional fold (i.e., the helix−turn−helix DNA binding motif) (*8*).

The three-dimensional solution structures of the wild-type vnd/NK-2[1] homeodomain in the absence of DNA and the homeodomain−DNA complex have been reported previously (*9*, *10*). Structures for other homeodomain−DNA complexes, determined primarily by X-ray cystallography, have been published (*11*−*16*). A comparison of these results illustrates the degree of structural similarity among the various homeodomain−DNA complexes. For example, residues in specific positions (i.e., 8, 16, 20, 26, 34, 35, 38, 40, 45, 48, and 49) across all the classical homeodomains typically are hydrophobic and make up the core of the protein. Conserved residues in positions 5, 47, 50, and 51, with few exceptions, make base specific contacts with the DNA. In the case of

‡ The structure of the A35T mutant vnd/NK-2 bound to its cognate DNA has been deposited with the Protein Data Bank as entries 1QRY and RCSB009193. The resonance assignments for the mutant protein are virtually complete. These assignments have been deposited as BMRB entry 4368 with the BioMagResBank (http://www.bmrb.wisc.edu).

* To whom correspondence should be addressed: 50 South Dr., Bethesda, MD 20892. Phone: (301) 496-3341. Fax: (301) 402-3405. E-mail: jafer@helix.nih.gov.

§ Laboratory of Biophysical Chemistry, National Heart, Lung and Blood Institute, National Institutes of Health.

|| Soong Sil University.

⊥ These authors contributed equally to this work.

@ Current address: Department of Chemistry and Chemical Biology, Cornell University, Ithaca, NY 14853.

Laboratory of Biochemical Genetics, National Heart, Lung and Blood Institute, National Institutes of Health.

+ Current address: Department of Biotechnology, Yonsei University, Bioinformatics and Molecular Design Research Institute, Seoul 120-749, Republic of Korea.

[1] Abbreviations: vnd, ventral nervous system; NK, Nirenberg and Kim; HMQC, heteronuclear multiple-quantum coherence; HSQC, heteronuclear single-quantum coherence; NOE, nuclear Overhauser effect; DGSA, distance geometry-simulated annealing.

10.1021/bi030116i CCC: $25.00
Published on Web 10/09/2003

the vnd/NK-2 homeodomain, L7 and Y54 also contact the DNA in the minor groove and major groove, respectively, and are responsible for the recognition of the unusual DNA consensus sequence that contains a 5′-CAAG-3′ sequence as part of the core rather than the canonical 5′-TAAT-3′ sequence (*8*). Other residues with positively charged side chains show electrostatic interactions with the DNA and contribute to the binding affinity. Current evidence suggests that changes of even the variable residues in a given homeodomain often result in abnormal development or disease (*7*). The hypothesis is that any amino acid residue change that alters the structure of any particular homeodomain or its interaction with its DNA in the proper functional context can result in genetic disease or cause disruption of normal development.

Various genetic diseases and developmental abnormalities have been mapped to numerous single-base mutations in the homeobox for numerous species, including humans, where these mutations often translate to single amino acid residue replacements in the homeodomain (*17*, *18*). Such single-residue replacements can result in a structural change in the homeodomain, a modification of the physical properties such as the "melting" temperature, or an alteration in the affinity and target specificity for the DNA (*19*−*21*). The relationship between these changes and the resulting implication for the understanding of alterations in transcriptional control is of considerable current interest.

The characterization of a number of vnd mutant alleles that produce transcriptional defects in early embryogenesis and result in embryonic lethality has been reported (*22*). One of these lethal vnd mutants was shown to encode the homeodomain protein with a single amino acid residue substitution in position 35 of the homeodomain, where alanine is replaced with threonine. Under conditions where the wild-type homeodomain is folded, the alanine side chain is partially surface exposed (*9*, *10*). Furthermore, only alanine and serine are found at position 35 in functional homeodomains (*7*). The absence of threonine at position 35 in any of the many homeodomains that have been found thus far suggests that its presence in that position is functionally detrimental. The question of the relation between the structure or the physical properties of the mutant homeodomain and improper transcriptional regulation thus arises. It was shown recently that the A35T mutant vnd/NK-2 homeodomain is unable to adopt a folded three-dimensional structure free in solution (*20*). The affinity of this mutant homeodomain for the consensus vnd/NK-2 target DNA, which contains the 5′-CAAGTG-3′ site, is reduced by a factor of 50 relative to that of the wild-type analogue (*20*). This reduction in binding affinity occurs even though in the structure of the wild-type homeodomain, the side chain of the residue in position 35 is partially surface exposed and does not contact the DNA. As a further examination of the structural implications of the placement of threonine in position 35, we describe the three-dimensional structure of the A35T mutant vnd/NK-2 homeodomain in its DNA-bound form.

MATERIALS AND METHODS

Preparation of the Uniformly ^{15}N-Labeled and ^{13}C- and ^{15}N-Labeled Mutant A35T vnd/NK-2 Homeodomain. The site-directed mutation, expression from the pET-15b vector in *Escherichia coli*, and purification of an 80-amino acid residue protein that encompasses the A35T vnd/NK-2 homeodomain were carried out as described previously (*20*). The singly ^{15}N-labeled protein was expressed in Martek Biosciences Corp. 9-N medium and the doubly ^{15}N- and ^{13}C-labeled protein in Martek 9-CN medium. The purification process is same as that for the unlabeled protein described previously, and involves loading the crude fraction on a Ni^{2+} affinity column. Both preparations were further purified by reverse-phase HPLC. The purity of the protein was confirmed by gel electrophoresis, as well as by mass spectroscopy (*37*) and NMR. The ^{15}N and ^{13}C enrichment of the uniformly labeled proteins was found to be 96.4% by mass spectroscopy. A yield of ∼13 mg of purified protein from 1 L of the medium was obtained.

The preparation of the A35T vnd/NK-2−DNA complex was reported previously (*20*). Both 16-mer DNA single strands (5′-ACAGCCACTTGACACA-3′ and 5′-TGTGTCAAGTGGCTGT-3′) containing the vnd/NK-2 target site were synthesized and purified by Midland Certified Reagent Co. The two single-strand segments were annealed following initial heating to 95 °C to form the double-strand DNA. The protein was then titrated slowly into the DNA solution to form the mutant homeodomain−DNA complex. The DNA:protein stoichiometry was adjusted to be 1:0.9 to ensure that all of the protein is bound to the unlabeled DNA. The pH of the samples was adjusted to 6.8. The concentration of all samples was ∼0.7 mM. Three separate samples were prepared in Shigemi NMR tubes containing sample volumes adjusted to 250 μL, two containing the uniformly doubly ^{15}N- and ^{13}C-labeled mutant homeodomain in 90% H_2O and 10% ^2H_2O and in 100% ^2H_2O, and one sample containing the uniformly ^{15}N-labeled mutant homeodomain in 90% H_2O and 10% ^2H_2O.

NMR Spectroscopy. All measurements were performed at 35 °C on a Bruker AMX600 spectrometer equipped with a triple-resonance probe and a single *z*-axis gradient amplifier. Gradient pulses were generated using a home-built gradient amplifier. All pulse experiments were implemented with pulse field gradients for coherence selection, and suppression of the strong water signal was accomplished using WATERGATE (*38*). Except when specified otherwise, all experiments were carried out on a 0.7 mM sample of either the uniformly singly ^{15}N- or doubly ^{15}N- and ^{13}C-labeled vnd/NK-2 homeodomain dissolved in 90% H_2O and 10% ^2H_2O. The concentration was restricted to 0.7 mM because of the limited solubility of the A35T mutant vnd/NK-2 homeodomain−DNA complex. A two-dimensional (2D) ^{15}N HSQC spectrum and the triple-resonance three-dimensional (3D) CBCANH and CBCA(CO)NH spectra were used to obtain the sequence specific chemical shift assignments for the backbone amide nitrogen and amide proton resonances (*39*, *40*) as well as those of the α- and β-carbon atoms (*41*). The spectral parameters for the HSQC experiment were as follows: 128* (t_1) × 512* (t_2) data points and spectral widths (acquisition times) of 1848.4 Hz in F_1 (69.2 ms) and 9090.9 Hz in F_2 (56.3 ms), with States quadrature detection in the t_1 dimension. For the 3D CBCANH experiment, the spectral parameters were as follows: 52* (t_1) × 20* (t_2) × 512* (t_3) data points and spectral widths (acquisition times) of 8445.9 Hz in F_1 (6.2 ms), 1849.1 Hz in F_2 (10.8 ms), and 9090.9

Hz in F_3 (56.3 ms), with States quadrature detection in the t_1 and t_2 dimensions. For the 3D CBCA(CO)NH experiments, the parameters were the same except that the width in F_2 was 3698.2 Hz (5.4 ms). A 3D HBHA(CO)NH experiment was used for the chemical shift assignments of the α- and β-proton resonances (*42*). The spectral parameters were as follows: 49* (t_1) × 20* (t_2) × 384* (t_3) data points and spectral widths (acquisition times) of 3759.4 Hz in F_1 (13.0 ms), 1855.3 Hz in F_2 (10.8 ms), and 9090.9 Hz in F_3 (42.2 ms), with States quadrature detection in the t_1 and t_2 dimensions. The remaining side chain carbon and proton assignments were obtained with a 3D HCCHTOCSY experiment on a 0.7 mM sample of the vnd/NK-2 homeodomain dissolved in 100% ^2H_2O (*43*). The spectral parameters were as follows: 64* (t_1) × 24* (t_2) × 384* (t_3) data points and spectral widths (acquisition times) of 4000.0 Hz in F_1 (16.0 ms), 3018 Hz in F_2 (8.0 ms), and 6024.1 Hz in F_3 (63.7 ms), with States quadrature detection in the t_1 and t_2 dimensions. A 3D HNHA experiment was carried out to determine the $^3J_{HNH\alpha}$ coupling constants (*44*). The spectral parameters were as follows: 47* (t_1) × 64* (t_2) × 512* (t_3) data points and spectral widths (acquisition times) of 1231.5 Hz in F_1 (38.2 ms), 4166.7 Hz in F_2 (15.4 ms), and 9090.9 Hz in F_3 (56.3 ms), with States quadrature detection in the t_1 and t_2 dimensions. A four-dimensional (4D) $^{15}N-^{13}C$-edited HMQC-NOESY-HSQC experiment was carried out to obtain some of the distance restraints and to resolve ambiguities in some of the resonance assignments obtained above (*45*). The spectral parameters were as follows: 16* (t_1) × 50* (t_2) × 24* (t_3) × 512* (t_4) data points and spectral widths (acquisition times) of 3017.5 Hz in F_1 (5.3 ms), 5399.6 Hz in F_2 (9.3 ms), 1582.3 Hz in F_3 (15.2 ms), and 9090.9 Hz in F_4 (56.3 ms), with States quadrature detection in the t_1, t_2, and t_3 dimensions. A ^{15}N-edited 3D NOESY-HSQC experiment with water flipback was carried out to obtain additional backbone distance restraints from weak cross-peaks and to observe cross-peaks to DNA (*24*). The spectral parameters were as follows: 128* (t_1) × 32* (t_2) × 512* (t_3) data points and spectral widths (acquisition times) of 5700.0 Hz in F_1 (22.5 ms), 1520.5 Hz in F_2 (21.0 ms), and 8333.3 Hz in F_3 (61.4 ms), with States-TPPI quadrature detection in the t_1 and t_2 dimensions. To obtain primarily side chain distance restraints, a 4D $^{13}C-^{13}C$-edited HMQC-NOESY-HSQC spectrum was recorded (*46*). The spectral parameters were as follows: 16* (t_1) × 64* (t_2) × 16* (t_3) × 256* (t_4) data points and spectral widths (acquisition times) of 3125.0 Hz in F_1 (5.1 ms), 5263.2 Hz in F_2 (12.2 ms), 3125.0 Hz in F_3 (5.1 ms), and 6024.1 Hz in F_4 (42.5 ms), with States quadrature detection in the t_1, t_2, and t_3 dimensions. For all NOESY experiments, the mixing time (τ_{mix}) was 100 ms.

Cross-Peak Intensity and Distance Restraints. Calibration of the NOESY cross-peak intensities was accomplished using the amide proton distances of residues in well-defined helical segments and the known distance between $H^{\epsilon 1}$ and $H^{\delta 2}$ of W48 (*25*). Distances between backbone amide protons and other protein protons were determined from the 4D $^{15}N-^{13}C$-edited HMQC-NOESY-HSQC and the 3D ^{15}N-edited NOESY-HMQC experiments (τ_{mix} = 100 ms). Distances between protons attached to ^{13}C were obtained from the 4D ^{13}C-edited HMQC-NOESY-HSQC experiment. For the ^{13}C-edited spectrum, cross-peak intensities of geminal methylene protons were calibrated using the corresponding fixed distances defined by the covalent geometry. Log−log fits to the cross-peak intensities were performed to judge consistency, as described previously (*9*). From these cross-peak intensities, a continuous set of interproton distance restraints was generated. The strategy employed here differs somewhat from that used for the determination of the structure of the wild-type vnd/NK-2 homeodomain−DNA complex (*9*). Because of the low solubility of the complex, the majority of protein−DNA cross-peaks could not be observed.

Table 1: Comparison of $^3J_{HNH\alpha}$ (Hertz) for Residues 23−28, 38−41, and 43

residue	wild type	A35T	residue	wild type	A35T
Q23	6.9	6.5	I38	9.4	8.8
R24	5.5	5.8	R39	5.2	5.4
Y25	5.5	7.3	L40	7.8	8.1
L26	8.7	5.9	T41	6.1	4.7
S27	8.7	6.3	T43	4.8	4.8
A28	4.8	3.1			

All spectra were processed with NMRPipe with linear prediction in the t_1 dimension for 2D spectra, in the t_1 and t_2 dimensions for 3D spectra, and in the t_1-t_3 dimensions for the 4D spectrum (*47*). NMRDraw and the pick picking program PIPP (*47*−*49*) were used on Silicon Graphics Indigo 2 and Octane workstations to aid cross-peak assignments of the 3D and 4D spectra. The program PROCHECK was used to analyze the structure statistics (*50*, *51*).

Structural Statistics. NOESY-derived distance restraints with and without protein backbone dihedral angle restraints obtained from the $^3J_{HNH\alpha}$ scalar couplings were used in the structure determinations. Also, for purposes of comparison, analogous computations using XPLOR 3.851 were carried out on the wild-type DNA-bound vnd/NK-2 homeodomain using the previously derived intraprotein distance, hydrogen bond, and dihedral angle restraints (*9*). Initially, 100 structures of the A35T mutant and the wild-type DNA-bound vnd/NK-2 homeodomain were embedded by distance geometry with the DGSA module of XPLOR using only the NOESY-derived distance restraints. Following the accepted procedures using XPLOR, these 100 structures were heated to 2000 K, followed by simulated annealing in 1000 steps of 0.003 ps (*28*). At this point, the 100 generated structures were subjected to preliminary refinement. A ramped asymmetric asymptotic soft potential function was used initially to avoid large forces associated with any significant NOE violations (*29*). A standard protocol was followed where, in each example, the 20 lowest-energy structures from the various sets of 100 structures then were chosen and subjected to heating to 3000 K, followed by simulated annealing (again using the DGSA module of XPLOR). In addition to the 1146 distance restraints for the A35T mutant homeodomain, structure refinements were carried out and the results compared with and without the experimental ϕ dihedral angle restraints for the structured region. In some cases, additional structural refinements were carried out to ensure that sets of structures were obtained with distance restraint violations of <0.3 Å and dihedral angle violations of $<5°$ (*28*). These structures were retained and used for statistical analysis (Table 2). As a check on the quality of the final sets of structures for the A35T mutant vnd/NK-2 homeodomain,

Table 2: Structural Statistics

no. of restraints	
distance	1146
dihedral angle (ϕ)	51[a]
mean rmsds from experimental restraints[b]	
distance (Å)	0.0236 (0.0179)
dihedral angle ϕ (deg)	0.475 (0.4416)
deviations from idealized covalent geometry[b]	
bonds (Å) (1403)	0.0052 (0.0040)
angles (deg) (3293)	0.78 (0.5837)
impropers (deg) (754)	1.85 (0.3929)
rmsds from mean structure (Å)[c]	
backbone atoms (N, C^α, C′, and O)	0.50 (0.327)
all heavy atoms	1.19 (0.955)
PROCHECK Ramachandran plot[c]	
most favored regions	68.9% (71.1%)
additionally allowed regions	24.4% (23.0%)
generously allowed regions	5.2% (5.2%)
disallowed regions	1.5% (1.5%)

[a] Only 43 dihedral restraints for the helix regions were used in the structure calculation. [b] Result of X-PLOR refinement. [c] The rmsds and PROCHECK results were calculated for residues 8−52. The N- and C-terminal parts of the protein are not well-defined because of the lack of long-range distance restraints. Values for the wild-type vnd/NK-2 homeodomain are given in parentheses. The ensembles of the 20 lowest-energy structures for both the A35T mutant and the wild-type homeodomain were used in the calculation. The values for the rmsd from the mean structures are to be compared with 0.49 and 0.89 Å, respectively, values obtained for the wild-type vnd/NK-2 homeodomain (*10*) in the absence of DNA.

comparisons were made for structures computed without the dihedral angle restraints for the loop region between helix I and helix II and for the turn region between helix II and helix III. No significant differences were observed for structures determined without the dihedral angle restraints, although, as expected, the rmsd values increased slightly. Furthermore, the unusual positive ϕ angle for residue R39 in other homeodomains is maintained for the A35T mutant even without dihedral angle restraints. The distance restraint that appears to be most critical for the positive ϕ angle for residue R39 is the one between the amide protons of residues L37 and R39.

On the basis of the experimental restraints, the mutant homeodomain is well-ordered with rmsd values about the mean coordinate, for residues from F8 through H52, of 0.50 Å for the backbone atoms and 1.19 Å for all heavy atoms. The corresponding XPLOR structure calculations for the wild-type homeodomain gave rmsd values of 0.33 Å for the backbone atoms and 0.96 Å for all heavy atoms [to be compared with values of 0.32 and 0.81 Å, respectively, for the wild type calculated simultaneously with the DNA (*9*)]. The absence of reliable restraints (due to low solubility) between both the N-terminal arm (residues 1−9 of the homeodomain) and the C-terminal portion of helix III (residues 53−60 of the homeodomain) with the DNA limited our ability to define the structure of these parts of the A35T mutant vnd/NK-2 homeodomain. The results obtained for the well-ordered region of the A35T mutant vnd/NK-2 homeodomain bound to DNA were used to generate the rms deviations reported in Table 2.

MD Simulations. Simulations were carried out using the InsightII/Discover (2.9.5) program package (*52*) that contains a free energy perturbation method with a consistent valence force field (CVFF) (*53*). To calculate the total hydration free energy change upon going from the wild-type to the A35T mutant homeodomain, the FDTI (finite difference thermodynamic integration) method was employed (*52*). Model structures used to calculate the free energy difference, $\Delta\Delta G^\circ_{300}$, were solvated in a 58.0 Å × 45.0 Å × 50.0 Å box of water.

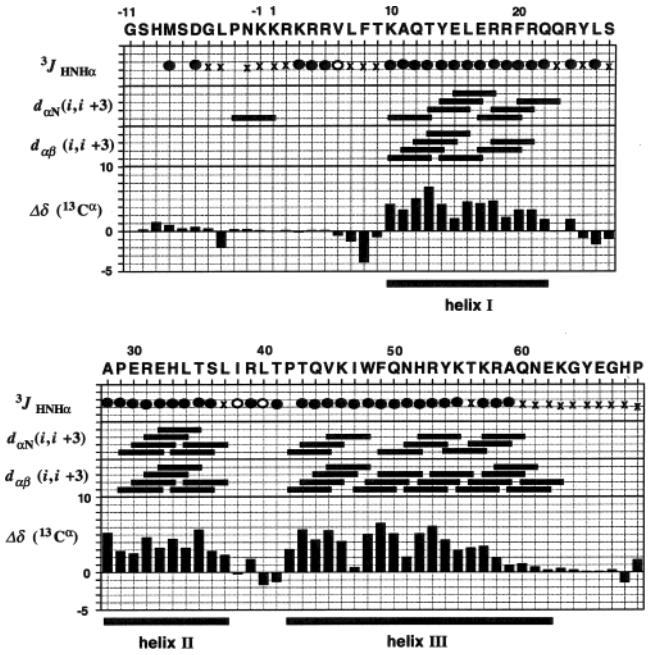

FIGURE 1: Amino acid sequence and numbering (top) and summary of the sequential NOE interactions, backbone $^3J_{HNH\alpha}$ coupling constants, and $^{13}C^\alpha$ chemical shift differences from random coil values that were used to characterize the secondary structure of the A35T vnd/NK-2 homeodomain. Coupling constants of <6.5 Hz are represented with filled circles and coupling constants of >6.5 Hz with empty circles, and x indicates that the couplings were not measurable.

RESULTS

NMR Spectroscopy. The A35T mutant vnd/NK-2 homeodomain binds tightly to the vnd/NK-2 DNA consensus sequence but with an affinity that is reduced by a factor of 50 compared to that seen for the wild-type analogue ($K_d = 2 \times 10^{-10}$ M) (*20*, *23*). The sequence of the 80-amino acid residue protein that was used in this study and that encompasses the homeodomain is shown in Figure 1. High-field proton resonances above 0.6 ppm (spectra not shown) that are characteristic for the formation of a hydrophobic core are observed (*20*). The positions of these resonances are quite similar to those found for the wild-type DNA-bound homeodomain.

The backbone sequential resonance assignments are complete except for the N-terminal glycine residue. Some of the faster exchanging side chain amine proton resonances could not be assigned. Overall, the chemical shifts of ∼95% of the side chain resonances have been assigned unambiguously. Many of the chemical shifts, ^{15}N, ^{13}C, and ^1H, of the A35T mutant homeodomain (pH 6.8) correspond quite well to those of the wild-type DNA-bound protein (*9*). In particular, this similarity in chemical shifts holds for those resonances whose side chains were shown to contact the DNA in the wild-type analogue. Four NOESY cross-peaks originating from the side chain NH_2 resonances of N51 (Figure 2) and R5 (data not shown) are seen at frequencies essentially identical

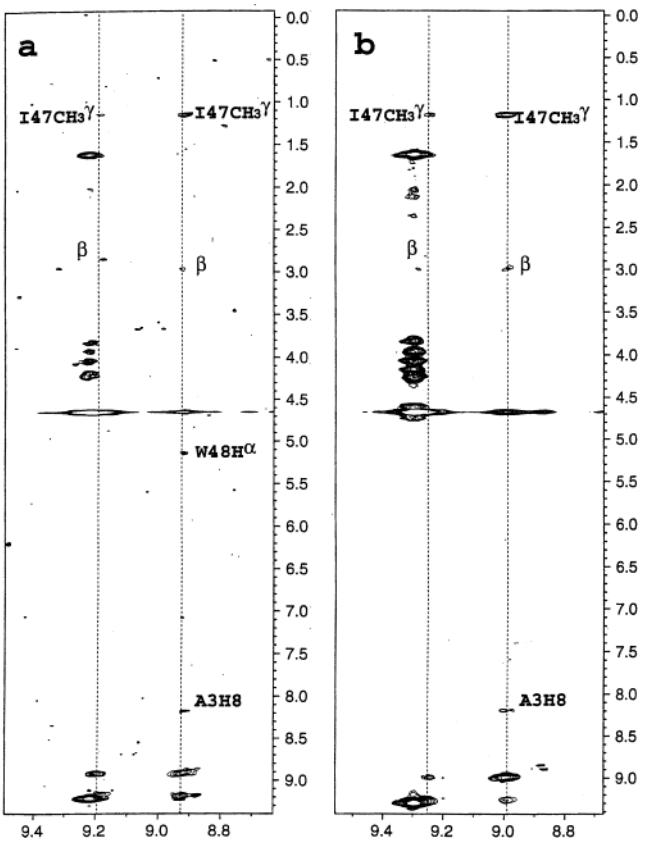

FIGURE 2: N51 side chain NH_2 resonances (indicated by vertical broken lines) and cross-peaks from the ^{15}N-edited 3D NOESY-HSQC spectra for mutant A35T (a) and wild-type vnd/NK-2 (b) homeodomains. Several important cross-peaks are labeled, including the cross-peak between the NH_2 (E) proton and the A3H8 proton of the DNA (*9*).

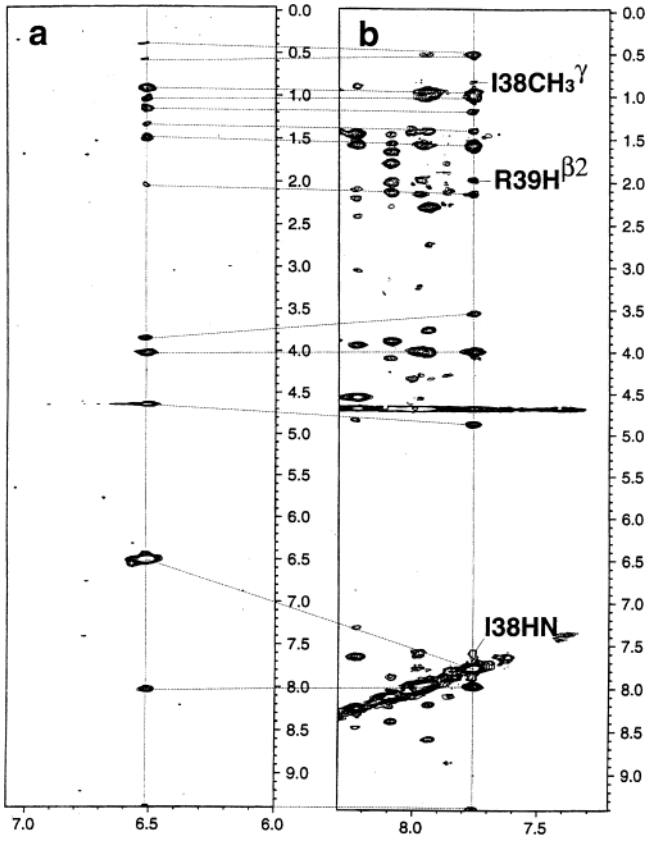

FIGURE 3: L40 NH resonance (indicated by a vertical solid line) and cross-peaks from the ^{15}N-edited 3D NOESY-HSQC spectra for mutant A35T (a) and wild-type vnd/NK-2 (b) homeodomains. Corresponding resonances in the spectra are connected by dotted lines.

to those found for the wild-type vnd/NK-2 with the DNA, i.e., one from the amide NH_2 of N51 with A3H8 and three from the guanidinium NH and NH_2 of R5, two of which are with A1H2 and one of which is with C2H3′. The invariant N51 residue makes a critical adenine base contact in all of the reported structures of the homeodomains (*8*), and on the basis of analogous chemical shifts, this contact with DNA in the A35T mutant homeodomain is maintained. The amide shifts were obtained using a ^{15}N-edited 3D NOESY-HSQC experiment with water flipback that optimizes cross-peaks from resonances involving exchangeable protons (*24*). Proton chemical shifts for resonances of side chains that make base specific contacts with the DNA were compared between the wild-type and A35T mutant vnd/NK-2 homeodomains in the bound state, i.e., those of R5, L7, Y25, I47, Q50, N51, and Y54. The side chain shift differences here are less than 0.1 ppm, thus indicating similar protein−DNA contacts in both cases.

Notable shift differences between the wild-type and mutant homeodomain in the DNA-bound state are seen for the backbone amide proton resonances of I38, L40, V45, and Q50. In the mutant homeodomain, the resonance for L40 is shifted upfield by 1.27 ppm (Figure 3), whereas those for I38, V45, and Q50 are shifted downfield by 0.2−0.5 ppm (*20*). The H^{α} resonances of the A35T mutant homeodomain all are within 0.3 ppm of the wild-type values with the exception of that of Q23, which is shifted upfield by 0.70 ppm. The only significant changes in backbone ^{15}N resonances were for S36, which is shifted downfield by 5.50 ppm, and for L40, which is shifted upfield by ∼1.0 ppm relative to that of the wild-type homeodomain. All of the backbone C^{α} resonances for the A35T mutant are within 0.5 ppm of the corresponding wild-type values, with the exception of that of T35. An important use of the chemical shift comparisons is to confirm structural differences found between the wild-type and mutant homeodomains.

The procedure used for the NOESY cross-peak intensity−distance calibration is described in Materials and Methods. For the structure calculations, a total of 1146 intraprotein distance restraints were obtained from the various NOESY experiments. This number is to be compared with 1591 upper bound intraprotein distance restraints obtained for the wild-type vnd/NK-2 homeodomain bound to DNA (*9*). The primary reason there are fewer restraints is the lower sensitivity due to the limited solubility of the mutant protein−DNA complex (0.7 mM). In addition to these distance restraints, 51 of the 72 available $^3J_{HNH\alpha}$ scalar couplings were converted into ϕ torsion angle restraints (from a 3D HNHA experiment) and used in the structure determination. The only significant differences in the ϕ torsion angle restraints (i.e., $^3J_{HNH\alpha}$) between the wild-type and A35T mutant homeodomain were observed for residues Y25, L26, S27, and A28 in the loop region between helix I and helix II and for T41 in the turn between helix II and helix III (see Table 1).

The amino acid sequence and a representation of the secondary structure of the A35T mutant vnd/NK-2 homeodomain bound to DNA that include $d_{\alpha N}(i, i + 3)$ and $d_{\alpha\beta}(i,$

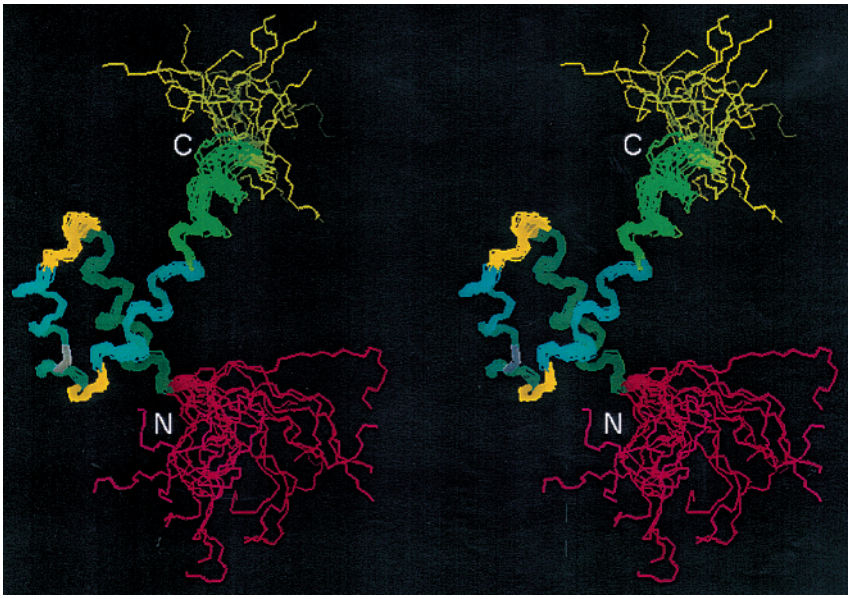

FIGURE 4: Stereoview of the superposition of 20 lowest-energy structures of the A35T vnd/NK-2 homeodomain bound to DNA. The well-ordered portions of the backbones of helices I−III ar shown in dark green. The T35 residue is show in gray. The N- and C-terminal ends of the protein are labeled.

$i + 3$), the backbone $^3J_{HNH\alpha}$ coupling constants, and $^{13}C^{\alpha}$ chemical shift differences relative to the standard random coil values are shown in Figure 1 (*25*−*27*). These results demonstrate the presence of three helical segments that is characteristic for the homeodomains (*7*) when the mutant homeodomain is bound to DNA. The presence of the three helical segments in the DNA-bound state contrasts with the inability of the mutant homeodomain to adopt a folded conformation free in solution (*20*).

Some differences in intraprotein NOE cross-peaks were observed between the wild-type and mutant homeodomains. For example, the cross-peak from one of the N51 amide NH_2 protons to Trp48 H^{α} is clearly observable in the spectrum of the A35T mutant−DNA complex, but can only be seen at a threshold much lower than that shown in the spectrum of the wild-type homeodomain−DNA complex (Figure 2). Another example is that of the cross-peak of the L40 amide proton with the β2 proton of R39, which is clearly observable in the spectrum of the wild-type analogue, but only barely visible at a significantly lower threshold in the spectrum of the mutant homeodomain−DNA complex (Figure 3).

Figure 4 shows a stereoview of the superimposition of the ensemble of 20 accepted low-energy structures. In analogy with the wild-type vnd/NK-2 (*9*, *10*) and other known homeodomains (*11*−*16*, *30*−*32*), the structure of the A35T mutant contains three helices. The loop between helix I and helix II is somewhat flexible, and there is a turn between helix II and helix III. The similarities of the side chain chemical shifts of the A35T mutant compared to the wild-type homeodomain for the residues in the N-terminal arm and in the region from P42 to T56 suggest that helix III and the N-terminal arm are inserted into the major and minor grooves of the DNA, respectively, which is analogous to other reported homeodomain−DNA structures (*9*). The C-terminal portion of helix III for the A35T mutant is not as well defined as that of the wild type in the DNA-bound state, presumably because of the lack of protein−DNA restraints rather than to any inherent mobility.

The PROCHECK program was used to assess the quality of the structure of the A35T mutant. In addition, comparison was made with the wild-type homeodomain, where both structures were determined using XPLOR (Table 2). The property comparisons for the A35T mutant and the wild-type homeodomains were quite similar, which is an indication that the qualities of the structures of the A35T mutant and wild-type vnd/NK-2 homeodomains are comparable.

Structural Analysis. Figure 1 shows the backbone *J* coupling $^3J_{HNH\alpha}$, the $d_{\alpha N}(i, i + 3)$ and $d_{\alpha\beta}(i, i + 3)$ distance restraints, and a histogram of the backbone $^{13}C^{\alpha}$ chemical shift differences (from random coil values) characteristic of protein secondary structures (*25*−*27*). The three helices are the same in position and are as long as those seen in the wild-type vnd/NK-2 homeodomain bound to DNA (*9*). Both the N-terminal region and the C-terminal portion after helix III exhibit no discernible secondary structure. These regions do not show many long-range NOE restraints, and their $^{13}C^{\alpha}$ chemical shifts are close to the canonical random coil values (*33*).

The backbone rmsd values between the average structures of residues F8−H52 of the wild-type and mutant homeodomains is 1.13 Å. Other comparisons between the A35T mutant and the wild-type vnd/NK-2 homeodomain were generated by superposition of residues K10−R21 of helix I or simultaneously of residues K10−R21 and K46−H52 of helix I and helix III, respectively. Figure 5 shows a comparison of the average structures of both the A35T mutant and the wild-type vnd/NK-2 homeodomains bound to DNA with superposition of residues K10−R21. The major local distortions between the A35T mutant and the wild-type homeodomains are found in the loop region between helix I and helix II and in the turn between helix II and helix III. Use of either superposition gave for residues Y25−A28 of the A35T mutant and wild-type structures backbone pairwise distances between the two structures of 2.06−3.16 Å. In addition, the structural distortions in the loop region result in larger distances with helix III for the A35T mutant.

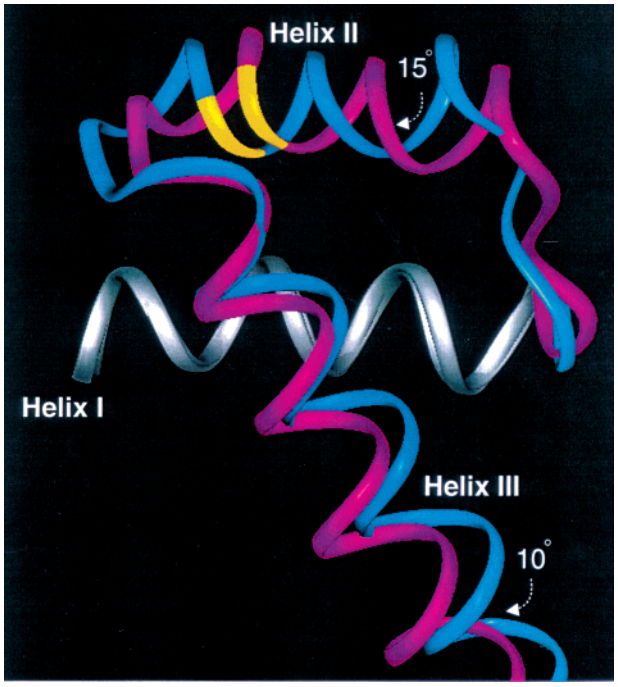

FIGURE 5: Superposition of helix I (residues 10−21, shown in white) of the average structure for the A35T mutant (pink) with the wild-type vnd/NK-2 (blue) homeodomain, highlighting the differences in the orientation of helices II and III. The backbones of A35 and T35 in each of the two structures are shown in yellow.

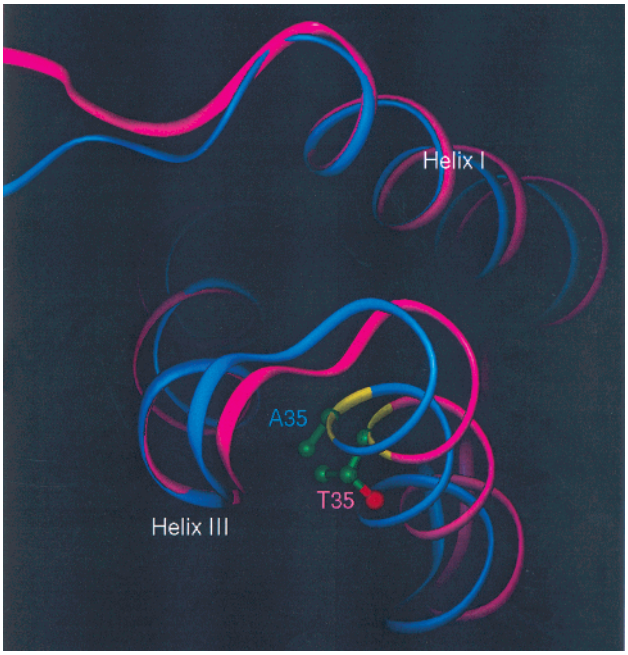

FIGURE 6: Backbone structures of A35T mutant vnd/NK-2 (pink) and wild-type vnd/NK-2 (blue) homeodomains. The side chains of T35 and A35 are displayed, showing the similar positioning of the methyl groups. The backbone regions for T35 and A35 are shown in yellow.

For example, the distance between the Y25 and H52 backbone amide nitrogen atoms is 13.1 Å for the A35T mutant, whereas it is 10.2 Å for the wild-type homeodomain. Solvation energies were calculated and compared for each residue of both proteins using Insight II. Three residues, F20, P29, and L40, exhibited measurable increases in solvation energies. Of these, F20 and L40 exhibited increases of a factor of ~2 in hydrophobic surface area. Such an increase in the extent of hydrophobic exposure is supported by the observed lower solubility of the A35T vnd/NK-2 homeodomain−DNA complex in water.

The distance between the backbone amide proton of L40 and the amide oxygen of I38 is 2.77 Å, whereas for the wild-type homeodomain, this distance is 3.35 Å. The backbone conformation for residues I38−L40 in the A35T mutant resembles a γ-turn (*34*), in contrast to the conformation of the turn region for the wild-type homeodomain (*9*). The presence of a second amide oxygen atom so close to the L40 amide proton in the A35T mutant homeodomain is consistent with and may provide a partial explanation for the large upfield shift (1.27 ppm) seen for the backbone amide proton of L40 in the A35T mutant relative to that of the wild-type homeodomain (*20*). In addition, the distance between the amide oxygen of residue 35 and the amide proton of residue 40 is 2.98 Å in the A35T mutant, whereas the corresponding distance is 2.48 Å in the wild-type homeodomain and is consistent with other (i, $i-5$) hydrogen bonds found in the turn regions of other homeodomains. The distance of 2.98 Å for the A35T mutant is at the upper limit for hydrogen bonds typically found in proteins (*35*).

The relative orientation of helix II (with respect to both helix I and helix III) in the A35T mutant vnd/NK-2 differs significantly from that found for the wild-type vnd/NK-2. Figure 5 highlights the relative orientation difference (~15°) of helix II between the A35T mutant and wild-type vnd/NK-2. The origin of this structural distortion seems, at least in part, to be a result of the steric packing due to the presence of the larger threonine side chain. Here the side chain methyl group of threonine appears to be in a similar position (Figure 6) in the hydrophobic core of the protein (i.e., the hydroxyl group points toward the surface of the protein) as the alanine methyl group in the case of the wild-type analogue. The net effect of the A35T mutation is to "push" or distort the C-terminal end of helix II away from helix I without significantly changing the structure of helix II. We found it surprising to see these distortions rather than to have this steric crowding compensated by small structural adjustments throughout helix II. A plausible hypothesis to explain the distortion of the axis of helix I relative to that of helix II is that the loop region between the two helices is sufficiently flexible to act as a hinge. The changes in $^3J_{HNH\alpha}$ (Table 1) and thus changes in the ϕ angles support this hypothesis. The orientation of helix III is also rotated slightly (less than 10°), increasing the distance between the C-terminal portion of the helix and the loop region. The hydrophobic core residue contacts from both the N-terminal portion of helix III (residues V45, W48, and F49) and the C-terminal portion (T56) are maintained, however, with this slight rotation apparently being compensated by a gradual bend occurring around residues 50−52. A gradual bend, rather than a more abrupt change, would be consistent with the observed values of $^3J_{HNH\alpha}$, which are practically unchanged in the mutant. Inherent in this bend might be differences in hydrogen bond lengths and angles that could explain some of the changes in backbone chemical shifts (*35*) seen in helix III of the A35T mutant, such as the 0.5 ppm change for the amide proton of Q50 (*20*).

The packing of the hydrophobic core of the A35T mutant vnd/NK-2 homeodomain is similar to that found for the wild-

type analogue, although the side chains of many of the residues involved in the hydrophobic core of the mutant seem to be displaced slightly relative to their respective backbone positions. This slight displacement appears to be global in nature, rather than involving only residues neighboring T35. One example is the side chain of L26, where the closest distance to the side chain of T35 is 7 Å. Both δ-methyl groups appear to be in analogous positions relative to the structure of the wild-type homeodomain, even though the backbone atoms of L26 are displaced in the A35T mutant. The δ-CH_3 resonances of L26 have relatively large upfield shifts, almost identical to those in the wild-type homeodomain, thereby indicating that they make up part of the hydrophobic core of both the A35T mutant and the wild-type analogue. It appears that a primary driving force in both the wild-type and A35T mutant homeodomains is the maintenance of the hydrophobic core. To maintain the hydrophobic core of the A35T mutant, there is an overall adjustment of the local side chain structures of the core residues in the mutant at the expense of distorting the backbone of the protein in the loop and turn regions. This backbone distortion is reflected then in the changes of the related backbone ϕ angles (Table 1).

DISCUSSION

The conformation of the A35T mutant vnd/NK-2 homeodomain bound to DNA shows many features that are similar to those of the wild-type vnd/NK-2 and of other homeodomains whose structure have been determined. Analogous orientation of the DNA is supported by the similar observation of cross-peaks between the side chain NH_2 resonances of N51 and R5 with the DNA and by very similar side chain chemical shifts (i.e., within 0.1 ppm) for those residues in the wild-type homeodomain that interact with the DNA (*9*). This evidence thus demonstrates that the wild-type and mutant homeodomains both bind the DNA in a similar way [i.e., the N-terminal arm contacts the DNA in the minor groove and helix III interacts with the DNA in the major groove (*9*), even though the change in position 35 from A to T resulted in a significant structural distortion].

The affinity of the mutant homeodomain for the same 5′-CAAGTG-3′ consensus DNA sequence is reduced by a factor of 50 compared to that for the wild-type protein (*20*). This lowered affinity corresponds to a reduction of ~2.4 kcal/mol in the free energy of binding. It is known from calorimetric studies that the values of $\Delta G°_{298}$ for unfolding of the wild-type homeodomain vary from 1.4 to 2.7 kcal/mol (*54*), depending on buffer and salt concentration. In an attempt to relate these values of $\Delta G°_{298}$ to the stability of the mutant homeodomain, the difference in the solvation free energies, $\Delta\Delta G^S_{300}$, between the wild type and A35T mutant was computed using the free energy perturbation module of the Discover program. The value of $\Delta\Delta G^S_{300}$ was calculated to be as large as 2.6 kcal/mol, with the A35T mutant being less stable than the wild-type homeodomain. Although such computations make numerous assumptions, this result implies that a difference in solvation free energy, even though it is only one component of the total free energy difference, could be sufficient in magnitude to destabilize the folded form of the A35T mutant homeodomain (*20*) in the absence of compensating factors. While inferring that the calculated value of $\Delta\Delta G^S_{300}$ can be translated into a corresponding decrease in the $\Delta G°$ for unfolding of the mutant homeodomain is attractive, thereby yielding a protein that is unable to fold, nevertheless one is limited to speculation based on the comparable values found for $\Delta G°_{298}$ and $\Delta\Delta G^S_{300}$ together with the structural similarities observed for both proteins in their respective DNA-bound states.

Finally, the question of the affinity of the A35T mutant vnd/NK-2 homeodomain for its cognate DNA being lower by a factor of 50 (2.4 kcal/mol) arises. Since binding of the A35T mutant to DNA starts from the unstructured homeodomain, one possibility is that the 2.4 kcal/mol reduction represents the energetic costs required to fold the protein before specific binding to DNA. The observed magnitude of $\Delta G°_{298}$ for unfolding of the wild-type homeodomain is in accord with this notion. An alternative explanation is based on the distortion of the structure of the mutant protein. While contacts with the DNA appear to be similar, the distortion could alter longer-range electrostatic forces such as those associated with helix dipole orientation or distances between protein and DNA charged groups. One example of the latter is for R24, where the distance $d_{C\beta-O2P}$ increases from 9.09 Å for the wild type to 11.35 Å for the mutant homeodomain.

The three-dimensional structure of and the various distortions in the mutant A35T vnd/NK-2 homeodomain bound to DNA are described. Although the modification involved only position 35, the structural ramifications of this alteration propagated throughout a large segment of the homeodomain. The structural changes observed for the A35T vnd/NK-2 homeodomain when bound to DNA are likely to be important factors related to or causing the early loss of embryonic viability in the mutant allele. Although the cellular events are not yet well understood and the question of degradation by endogenous proteases exists, the idea that a structural modification in the homeodomain would alter the geometry of the full-length protein and thus affect the transcriptional activation process is appealing. Such distortions would be expected to significantly alter protein−protein interactions as well as the lifetime of the transcriptional activation complex, both being necessary for proper regulation of downstream target genes (*55*).

The observation that alanine and serine are the only residues found in functional homeodomains (*7*) now can be understood in terms of the structural requirements associated with position 35 of the homeodomain. On the basis of our results, we conclude that replacement of alanine or serine with other amino acid residues would result in significant structural distortions. As an example, it has been shown that the presence of valine at position 35 in a mutant homeodomain is strongly correlated with genetic disease (*36*). Presumably, this mutant homeodomain bound to DNA suffers from structural alterations analogous to those found in the study presented here.

ACKNOWLEDGMENT

We thank Dr. Nico Tjandra for helpful discussions and assistance in acquisition and processing of NMR data.

REFERENCES

1. Gehring, W. J., Affolter, M., and Burglin, T. (1994) Homeodomain proteins, *Annu. Rev. Biochem. 63*, 487−526.
2. McGinnis, W., and Krumlauf, R. (1992) Homeobox genes and axial patterning, *Cell 68*, 283−302.

3. Scott, M. P., Tamkun, J. W., and Hartzell, G. W., III (1989) The structure and function of the homeodomain, *Biochim. Biophys. Acta 989*, 25−48.
4. Francis-Lang, H., Price, M., Polycarpou-Schwartz, M., and Di Lauro, R. (1992) Cell-type specific expression of the rat thyroperoxidase promoter indicates common mechanisms for thyroid-specific gene expression, *Mol. Cell. Biol. 12*, 576−588.
5. Lyons, I., Parsons, L. M., Hartley, L., Li, R., Andrews, J. E., Robb, L., and Harvey, R. P. (1995) Myogenic and morphogenetic defects in the heart tubes of murine embryos lacking the homeo box gene Nkx2-5, *Genes Dev. 9*, 1654−1666.
6. Bhatia-Gaur, R., Donjacour, A. A., Sciavolino, P. J., Kim, M., Desai, N., Young, P., Norton, C. R., Gridley, T., Cardiff, R. D., Cunha, G. R., Abate-shen, C., and Shen, M. M. (1999) Role for NKx3.1 in prostate development and cancer, *Genes Dev. 13*, 966−977.
7. Duboule, D. (1994) *Guidebook to the Homeobox Genes*, Oxford University Press Inc., New York.
8. Gruschus, J. M., Tsao, D. H. H., Wang, L., Nirenberg, M., and Ferretti, J. A. (1997) Interactions of the vnd/NK-2 homeodomain with DNA by nuclear magnetic resonance spectroscopy: basis of binding specificity, *Biochemistry 36*, 5372−5380.
9. Gruschus, J. M., Tsao, D. H. H., Wang, L., Nirenberg, M., and Ferretti, J. A. (1999) The three-dimensional structure of the vnd/NK-2 homeodomain-DNA complex by NMR spectroscopy, *J. Mol. Biol. 288*, 529−545.
10. Tsao, D. H. H., Gruschus, J. M., Wang, L.-H., Nirenberg, M., and Ferretti, J. A. (1995) The 3-dimensional solution structure of the NK-2 homeodomain from *Drosophila*, *J. Mol. Biol. 251*, 297−307.
11. Hirsch, J. A., and Aggarwal, A. K. (1995) Structure of the even-skipped homeodomain complexed to AT-rich DNA: new perspectives on homeodomain specificity, *EMBO J. 14*, 6280−6291.
12. Jacobson, E. M., Li, P., Leon del Rio, A., Rosenfeld, M. G., and Aggarwal, A. K. (1997) Structure of the Pit-1 POU domain bound to DNA as a dimer: unexpected arrangement and flexibility, *Genes Dev. 11*, 198−212.
13. Kissinger, C. R., Liu, B., Martin-Bianco, E., Kornberg, T. B., and Pabo, C. O. (1990) Crystal structure of an engrailed homeodomain-DNA complex at 2.8 Å resolution: a framework for understanding homeodomain-DNA interactions, *Cell 63*, 579−590.
14. Li, T., Stark, M. R., Johnson, A. D., and Wolberger, C. (1995) Crystal structure of the MATA1/MAT-alpha-2 homeodomain heterodimer bound to DNA, *Science 270*, 262−269.
15. Qian, Y. Q., Otting, G., Billeter, M., Müller, M., Gehring, W., and Wüthrich, K. (1993) Nuclear-magnetic-resonance spectroscopy of a DNA complex with the uniformly C-13-labeled Antennapedia homeodomain and structure determination of the DNA-bound homeodomain, *J. Mol. Biol. 234*, 1070−1083.
16. Wolberger, C., Vershon, A. K., Liu, B., Johnson, A. D., and Pabo, C. O. (1991) Crystal structure of a MAT alpha-2 homeodomain-operator complex suggests a general model for homeodomain-DNA interactions, *Cell 67*, 517−528.
17. Schott, J., Benson, D. W., Basson, C. T., Pease, W., Silberbach, G. M., Moak, J. P., Maron, B. J., Seidman, C. E., and Seidman, J. G. (1998) Congenital heart disease caused by mutations in the transcription factor *NKX2-5*, *Science 281*, 108−111.
18. Boncinelli, E. (1997) Homeobox genes and disease, *Curr. Opin. Genet. Dev. 7*, 331−337.
19. Weiler, S., Gruschus, J. M., Tsao, D. H. H., Yu, L., Wang, L., Nirenberg, M., and Ferretti, J. A. (1998) Site-directed mutations in the vnd/NK-2 homeodomain-basis of variations in structure and sequence-specific binding, *J. Biol. Chem. 273*, 10994−11000.
20. Xiang, B., Weiler, S., Nirenberg, M., and Ferretti, J. A. (1998) Structural basis of an embryonically lethal single Ala → Thr mutation in the vnd/NK-2 homeodomain, *Proc. Natl. Acad. Sci. U.S.A. 95*, 7412−7416.
21. TuckerKellogg, L., Rould, M. A., Chambers, K. A., Ades, S. E., Sauer, R. T., and Pabo, C. O. (1997) Engrailed (Gln50 → Lys) homeodomain-DNA complex at 1.9 Å resolution: structural basis for enhanced affinity and altered specificity, *Structure 5*, 1047−1057.
22. Jiménez, F., Martin-Morris, L. E., Valasco, L., Chu, H., Sierra, J., Rosen, D. R., and White, K. (1995) *vnd*, a gene required for early neurogenesis of *Drosophila*, encodes a homeodomain protein, *EMBO J. 14*, 3487−3495.
23. Tsao, D. H. H., Gruschus, J. M., Wang, L.-H., Nirenberg, M., and Ferretti, J. A. (1994) Elongation of helix-III of the NK-2 homeodomain upon binding to DNA: a secondary structure study by NMR, *Biochemistry 33*, 15053−15060.
24. Gruschus, J. M., and Ferretti, J. A. (1998) ^{15}N-edited three-dimensional NOESY-HMQC with water flipback: enhancement of weak labile ^{1}H resonances of protein side chains contacting DNA, *J. Magn. Reson. 135*, 87−92.
25. Wüthrich, K. (1986) *NMR of Proteins and Nucleic Acids*, Wiley, New York.
26. Spera, S., and Bax, A. (1991) Empirical correlation between protein backbone conformation and C_α and C_β ^{13}C nuclear magnetic resonance chemical shifts, *J. Am. Chem. Soc. 113*, 5490−5492.
27. Wishart, D. S., and Sykes, B. D. (1994) The ^{13}C chemical-shift index: a simple method for the identification of protein secondary structure using ^{13}C chemical-shift data, *J. Biomol. NMR 4*, 171−180.
28. Brunger, A. A. (1992) *X-PLOR*, version 3.1, Yale University Press, New Haven, CT.
29. Nilges, M., Gronenborn, A. M., Brunger, A. T., and Clore, G. M. (1988) Determination of three-dimensional structures of proteins by simulated annealing with interproton distance restraints: application to crambin, potato carboxypeptidase inhibitor and barley serine proteinase inhibitor 2, *Protein Eng. 2*, 27−38.
30. Klemm, J. D., Rould, M. A., Aurora, R., Herr, W., and Pabo, C. O. (1994) Crystal-structure of the OCT-1 POU domain bound to an octamer site-DNA recognition with tethered DNA-binding modules, *Cell 77*, 21−32.
31. Tan, S., and Richmond, T. J. (1998) Crystal structure of the yeast MAT alpha 2/MCM1/DNA ternary complex, *Nature 391*, 660−666.
32. Wilson, D. S., Gunther, B., Desplan, C., and Kuriyan, J. (1995) High-resolution crystal-structure of a paired (PAX) class cooperative homeodomain dimer on DNA, *Cell 82*, 709−719.
33. Wishart, D. S., Bigam, C. G., Holm, A., Hodges, R. S., and Sykes, B. D. (1995) ^{1}H, ^{13}C and ^{15}N random coil NMR chemical shifts of the common amino acids. I. Investigations of nearest-neighbor effects, *J. Biomol. NMR 5*, 67−81.
34. Nemethy, G., and Printz, M. P. (1972) The γ Turn, a Possible Folded Conformation of the Polypeptide Chain. Comparison with the β Turn, *Macromolecules 5*, 755−758.
35. Sharma, Y., Kwon, O. Y., Brooks, B., and Tjandra, N. (2002) An *ab initio* study of amide proton shift tensor dependence on local protein structure, *J. Am. Chem. Soc. 124*, 327−335.
36. Blitner-Glindzicz, M., Turnpenny, P., Hoglund, P., Kaariainen, H., Sankila, E., van der Maarel, S. M., de Kok, Y. J. M., Ropers, H., Cremers, F. P. M., Pembrey, M., and Malcolm, S. (1995) Further mutations in *Brain 4* (POU3F4) clarify the phenotype in the X-linked deafness, DFN3, *Hum. Mol. Genet. 4* (8), 1467−1469.
37. Xiang, B., Ferretti, J., and Fales, H. M. (1998) Use of mass spectrometry to ensure purity of recombinant proteins: a cautionary note, *Anal. Chem. 70*, 2188−2190.
38. Piotto, M., Saudek, V., and Sklenar, V. (1992) Gradient-tailored excitation for single-quantum NMR-spectroscopy of aqueous solution, *J. Biomol. NMR 2*, 661−665.
39. Bodenhausen, G., and Ruben, D. J. (1980) Natural abundance nitrogen-15 NMR by enhanced heteronuclear spectroscopy, *Chem. Phys. Lett. 69*, 185−189.
40. Grzesiek, S., and Bax, A. (1992) An efficient experiment for sequential backbone assignment of medium-sized isotopically enriched proteins, *J. Magn. Reson. 99*, 201−207.
41. Grzesiek, S., and Bax, A. (1992) Correlating backbone amide and side chain resonances in larger proteins by multiple relayed triple resonance NMR, *J. Am. Chem. Soc. 114*, 6291−6293.
42. Grzesiek, S., and Bax, A. (1993) Amino acid type determination in the sequential assignment procedure of uniformly ^{13}C/^{15}N-enriched proteins, *J. Biomol. NMR 3*, 185−204.
43. Bax, A., Clore, G. M., and Gronenborn, A. M. (1990) ^{1}H−^{1}H correlation via isotropic mixing of ^{13}C magnetization, a new three-dimensional approach for assigning ^{1}H and ^{13}C spectra of ^{13}C-enriched proteins, *J. Magn. Reson. 88*, 425−431.
44. Vuister, G. W., and Bax, A. (1993) Quantitative *J* correlation: a new approach for measuring homonuclear three-bond $J_{(HNH\alpha)}$ coupling constants in ^{15}N-enriched proteins, *J. Am. Chem. Soc. 115*, 7772−7777.
45. Muhandiram, D. R., Xu, G. Y., and Kay, L. E. (1993) An enhanced-sensitivity pure absorption gradient 4D ^{15}N, ^{13}C-edited NOESY experiment, *J. Biomol. NMR 3*, 463−470.
46. Vuister, G. W., Clore, G. M., Gronenborn, A. M., Powers, R., Garrett, D. S., Tschudin, R., and Bax, A. (1993) Increased

resolution and improved spectral quality in four-dimensional $^{13}C/^{13}C$-separated HMQC-NOESY-HMQC spectra using pulsed field gradient, *J. Magn. Reson., Ser. B 101*, 210−213.
47. Delaglio, F., Grzesiek, S., Vuister, G. W., Zhu, G., Pfeifer, J., and Bax, A. (1995) NMRPipe: a multidimensional spectral processing system based on Unix pipes, *J. Biomol. NMR 6*, 277−293.
48. Garrett, D. S., Powers, R., Gronenborn, A. M., and Clore, G. M. (1991) A common sense approach to peak picking in two-, three-, and four-dimensional spectra using automatic computer analysis of contour diagrams, *J. Magn. Reson. 95*, 214−220.
49. Garrett, D. S., Gronenborn, A. M., and Clore, G. M. (1995) Automated and interactive tools for assigning 3D and 4D NMR spectra of proteins: CAPP, STAPP and PIPP, *J. Cell. Biochem. 71*, 21b.
50. Laskowski, R. A., MacArthur, M. W., Moss, D. S., and Thorton, J. M. (1993) PROCHECK: a program to check the stereochemical quality of protein structures, *J. Appl. Crystallogr. 26*, 283−291.
51. Laskowski, R. A., Rullmann, J. A. C., MacArthur, M. W., Kaptein, R., and Thornton, J. M. (1996) AQUA and PROCHECK-NMR: programs for checking the quality of protein structures solved by NMR, *J. Biomol. NMR 8*, 477−486.
52. Biosym Technologies, Inc. (1998) *InsightII(980)/Discover 2.9.5*, Molecular Modeling Software, San Diego.
53. Hagler, A. T., Lifson, S., and Dauber, P. (1979) Consistent Force Field Studies of Intermolecular Forces in Hydrogen-Bonded Crystals. 2. A Benchmark for the Objective Comparison of Alternative Force Fields, *J. Am. Chem. Soc. 101*, 5122−5130.
54. Gonzalez, M., Weiler, S., Ferretti, J. A., and Ginsburg, A. (2001) The vnd/NK-2 Homeodomain: Thermodynmaics of Reversible Unfolding and DNA: Binding for wild-type and with Residue Replacements H52R and H52R/T56W in Helix III, *Biochemistry 40*, 4923−4931.
55. Koizumi, K., Lintas, C., Nirenberg, M., Maeng, J.-S., Ju, J.-H., Mack, J. W., Gruschus, J. M., Odenwald, W. F., and Ferretti, J. A. (2003) Mutations that affect the ability of the vnd/NK-2 homeoprotein to regulate gene expression: Transgenic alterations and tertiary structure, *Proc. Natl. Acad. Sci. U.S.A. 100*, 3119−3124.

BI030116I